

Electronic structure of face-centered-tetragonal iron in ferromagnetic iron-copper multilayers

S. J. Lloyd and R. E. Dunin-Borkowski*

Department of Materials Science and Metallurgy, University of Cambridge, Cambridge CB2 3QZ, United Kingdom

(Received 20 May 1997; revised manuscript received 28 September 1998)

Three short-period coherent face-centered Fe/Cu multilayers are characterized using transmission electron microscopy and x-ray diffraction. Both the tetragonal distortion of the Fe and its electron structure are shown to depend on Fe-layer thickness, with the Fe expanded by up to 7% over its cubic lattice parameter. The effect of changes in electron structure on “strain” in short-period coherent multilayers is discussed.

[S0163-1829(99)05903-2]

I. INTRODUCTION

The properties of synthetic multilayers with individual layer thicknesses of a few nm or less can be controlled through the design of the layered structure. The electronic properties of semiconductors have been modified in this way,¹ and metallic multilayers have aroused similar interest for their elastic² and magnetic³ properties. Both the elastic moduli⁴ and the magnetic properties⁵ of ultrathin metal films are known to be correlated with changes in lattice spacing. It has been suggested that these lattice spacing changes are localized at interfaces,⁶ and that tetragonal metallic phases form as a result of elastic deformations associated with coherency strains.⁷ In this paper, an alternative possibility is considered: that structural distortions can result directly from changes in the electron structure of thin layers relative to the bulk metal. The atomic structure would then be as much a “property” determined by the electron structure as is magnetism.

Transmission electron microscopy will be used to characterize the compositions, lattice spacings, and electron structures of ferromagnetic Fe/Cu multilayers, in which the Fe is sufficiently thin to grow coherently on (001) Cu in a face-centered-tetragonal (fct) (Ref. 8) structure rather than the usual body-centered structure. The magnetic properties of face-centered-cubic (fcc) Fe, which can exist at room temperature in the form of small particles in a matrix such as MgO,⁹ are very sensitive to atomic spacing.¹⁰ Such fcc Fe particles are antiferromagnetic in Cu below 70 K,¹¹ whereas they are ferromagnetic in Cu-Au alloys,¹² in which they have a larger lattice spacing. Thin films of Fe exhibit a similar variety of structures and magnetic properties.¹³ A knowledge of the local atomic and electron structures of such layers is essential for tailoring their properties and for understanding effects such as giant magnetoresistance and magnetic anisotropy.¹⁴

II. EXPERIMENTAL DETAILS AND MAGNETIC PROPERTIES

Fe/Cu multilayers were deposited by magnetron sputtering¹⁵ onto freshly cleaved (001) NaCl. The multilayers were *single crystals* with coherent, flat layers, as illustrated by the schematic diagram in Fig. 1 and the TEM micrograph in Fig. 2. Three samples, whose structures are summarized in Table I, exhibited particularly strong 002 x-ray-diffraction intensity. Samples A, B, and C, which each

consisted of 100 repeat units on a 300-nm Cu buffer with a 150-nm Cu capping layer, were grown under identical conditions with similar periods Λ of ~ 3 nm and nominally two, four, and six atomic layers (AL's) of Fe, respectively. Cross-sectional TEM samples were prepared by floating the multilayers from their NaCl substrates in water, enclosing them in folding Cu grids and Cu plating, using a copper pyrophosphate solution. Sections of the plated multilayers were ground mechanically to wedge shapes before Ar-ion thinning to electron transparency.

Hysteresis curves were obtained from the multilayers (still attached to their NaCl substrates) using a vibrating sample magnetometer.¹⁶ Saturation magnetizations are shown in Fig. 3 for the range 10–300 K, and the magnetic properties are summarized in Table II. The magnetic properties of the multilayers are different both from each other and from room-temperature-stabilized face-centered-cubic Fe.¹¹ The multilayers are all ferromagnetic, although A is superparamagnetic at high temperatures. A and B are perpendicularly magnetized (their easy direction is [001]) and have similar Curie temperatures (less than that of C). A has the highest moment per Fe atom at 0 K.

III. LATTICE SPACINGS

X-ray diffraction cannot be used to determine the lattice spacing variation in the Fe/Cu multilayers directly without a

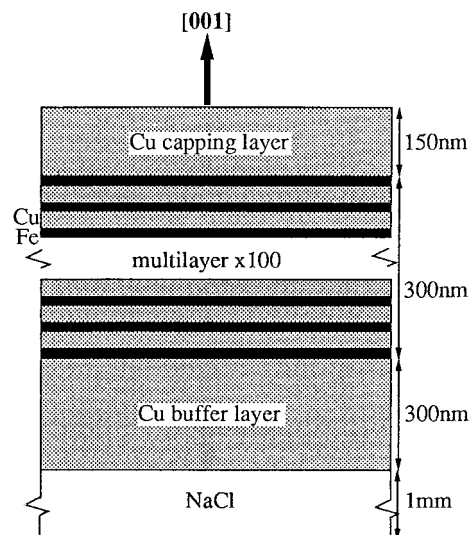


FIG. 1. Schematic diagram of multilayer structures.

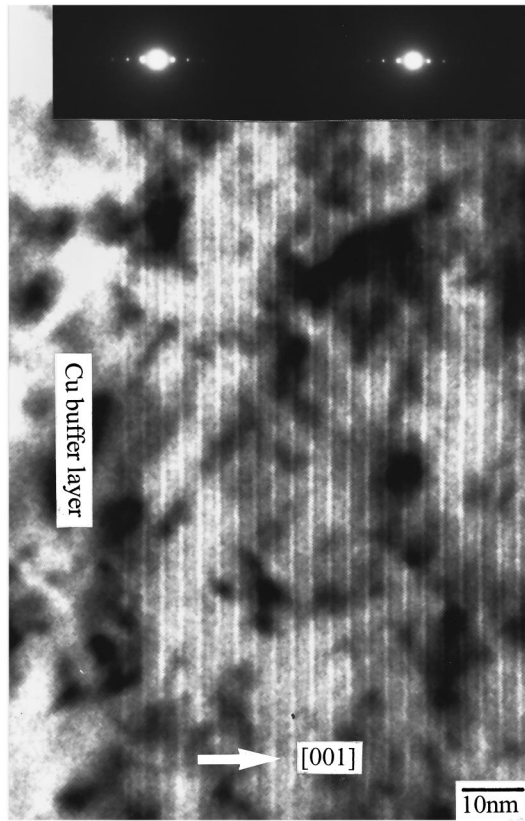


FIG. 2. Bright-field TEM micrograph of multilayer *B*, with diffraction pattern inset.

knowledge of the interface structure, since the high-angle superlattice intensities are affected by both parameters.¹⁷ It is, however, possible to determine *average* lattice spacings to high accuracy from x-ray traces such as that shown for multilayer *A* in Fig. 4. Such spacing measurements, which are summarized for all three samples in Table III, were compared with the predictions of continuum elasticity theory using two models. In the “slab” model the in-plane lattice parameter is constrained to that of the Cu buffer, the Cu within the multilayer remains cubic, and the strain in the tetragonal Fe is independent of layer thickness. In the “strain energy” model the multilayer is free from its substrate, the Cu and Fe are tetragonally distorted, and both the distortion and the common in-plane lattice parameter depend on the relative thicknesses of the layers. The equations for both models are given in Appendix A. Figure 5(a) shows the average lattice spacings predicted using anisotropic elastic constants for both Cu (Ref. 18) and fcc Fe,¹⁹ and lattice parameters of 0.3615 nm for Cu and 0.3585 nm for fcc Fe.²⁰ Both

TABLE I. Parameters describing Fe/Cu multilayer structures: w is the nominal thickness in each repeat unit in atomic layers (AL), and Λ is superlattice period determined from x-ray diffraction.

Sample	Nominal w_{Fe} (AL)	Nominal w_{Cu} (AL)	Number of repeats	Λ (nm)
A	2	15	100	3.19 ± 0.01
B	4	13	100	3.07 ± 0.005
C	6	9	100	2.80 ± 0.05

models predict that the average (002) spacing should decrease as the Fe content of the multilayer increases. The experimental spacings show the same trend, but are much greater than predicted by either model. Assuming that the nominal thicknesses of the Fe and Cu layers are approximately correct, the data provide a preliminary indication that the (002) spacings in the multilayers are inconsistent with predictions that incorporate bulk material properties. This is also apparent from Fig. 5(b), which shows that the Fe should be contracted along [001] relative to Cu, in contrast to the increased Fe(002) spacings inferred from the x-ray data on the assumption that the Cu remains cubic.

Attempts to determine the (002) lattice spacings directly using TEM techniques were unsuccessful. Dark-field rocking curves using high-order reflections verified that the Fe was expanded relative to Cu; however, the expansion could not be quantified as the deviation parameter could not be measured accurately.¹⁶ Nonaxial high-resolution images²¹ could not distinguish between model structures with the Fe(002) spacing contracted and expanded relative to Cu. Convergent beam electron diffraction is also unable to provide accurate measurements because the lattice spacings vary too rapidly.²²

IV. MEASUREMENT OF MEAN INNER POTENTIAL PROFILES

The mean inner potential of a sample measured in TEM (Refs. 23–25) is

$$V_0 = \left(\frac{h^2}{2\pi m_e e \Omega} \right) \sum_{\text{unit cell}} f_{\text{el}}(0), \quad (1)$$

where h is Planck’s constant, m_e and e are the rest mass and charge of an electron, Ω is the unit-cell volume and $f_{\text{el}}(0)$ is the electron scattering factor of each atom at zero scattering angle.²⁶ The potential difference ΔV between adjacent Fe and Cu layers is then the difference between the values of V_0 in the two materials and is given by the equation

$$\Delta V = \frac{4k}{a_x^2} \left(\frac{f_{\text{el}}^{\text{Fe}}(0)}{a_z^{\text{Fe}}} - \frac{f_{\text{el}}^{\text{Cu}}(0)}{a_z^{\text{Cu}}} \right), \quad (2)$$

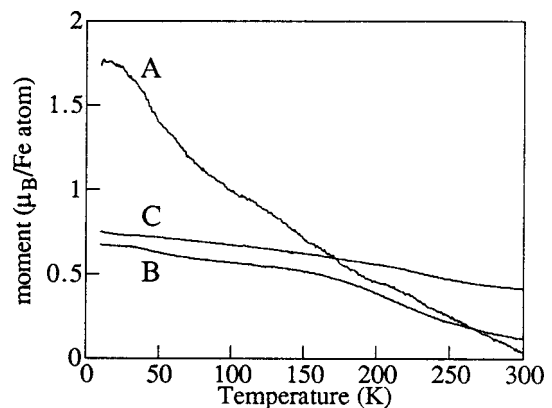


FIG. 3. Saturation magnetization (M_s) as a function of temperature.

TABLE II. Magnetic properties of multilayers, assuming the Fe layer thicknesses in Table I. M_S is the saturation magnetization, T_C is the Curie temperature, K is the anisotropy energy measured at 70 K and H_C is the maximum coercive field at 70 K.

Sample	M_S (0 K) $\mu_B/\text{Fe atom}$	T_C (K)	Magnetic easy axis	K (70 K) (kJ m^{-3})	H_C (kA m^{-1})
A	1.7	~ 300	$\parallel[001]$	420	15
B	0.7	~ 300	$\parallel[001]$	<470	200
C	0.8	$\sim 350\text{--}450$	$\perp[001]$	160	75

where $k=4.7878\times 10^{-19}$ V m², a_x is the common in-plane lattice parameter, and a_z^{Fe} and a_z^{Cu} are the lattice parameters of the Fe and Cu layers, respectively, parallel to [001].

Fresnel contrast analysis in the TEM can be used to determine the mean inner potential profile across the multilayer.²⁷ A through-focal series of images of the layer, which is typically examined in cross section at a weakly diffracting orientation, is obtained using a small objective aperture and coherent illumination. The contrast is compared with simulations that describe the variation in V_0 underlying that of the atoms, which determines the form of the Fresnel fringes visible at the interface as a function of defocus. To first order, the spacing and contrast of the fringes are sensitive to the width and the shape of the potential profile, respectively.²⁷ Energy-filtered imaging now allows inelastic scattering to be removed from images, and hence the image contrast to be interpreted quantitatively. The remaining primary source of error is the accuracy to which the specimen thickness of each region of interest can be measured.

Experimental Fresnel defocus series were obtained at 397 kV using a JEOL 4000FX TEM ($C_S=2.0$ mm, $C_C=1.4$ mm) equipped with a post-column Gatan imaging filter. The samples were oriented a few degrees from [100] with the layers parallel to the incident electron beam. An energy-selecting slit of width 10 eV was centered on the zero-loss peak, and the objective aperture semiangle was 3.4 mrad (corresponding to an Airy disc radius of 0.29 nm). Images were captured on a 1024 \times 1024 pixel CCD camera at a sampling density of 0.049 nm/pixel, and the point spread function of the detector was deconvoluted from each image.

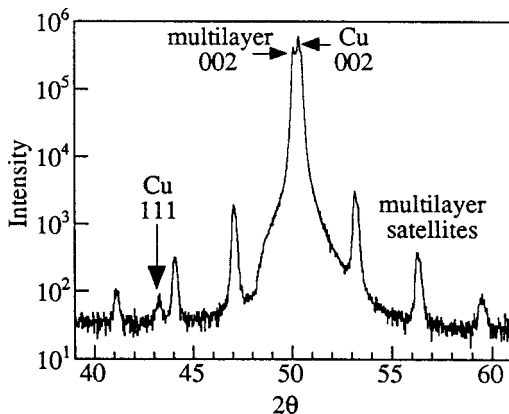


FIG. 4. X-ray-diffraction trace from multilayer A. 002 reflections from multilayer (at lower diffraction angle) and Cu buffer and capping layers are visible.

TABLE III. X-ray measurements of average (001) spacing in multilayers and buffer layers. (The error in each value is $\sim\pm 0.0002$ nm).

Sample	Buffer (nm)	Multilayer (nm)
A	0.3623	0.3640
B	0.3617	0.3638
C	0.3617	0.3629

The specimen thickness t could not be determined using weak beam thickness fringes because of local foil bending, and was obtained instead from the ratio of intensities in unfiltered and energy-filtered images (denoted I_{tot} and I_{el}) using the equation²⁸

$$(t/\lambda_{\text{in}}) = \ln(I_{\text{tot}}/I_{\text{el}}), \quad (3)$$

where λ_{in} is the total inelastic mean free path. A value for λ_{in} of 130 nm was chosen, and the justification for this choice is given in Appendix B. However, care is required here because a value of t determined using Eq. (3) contains contributions from both the crystal and amorphous surface layers such that $t \approx t_{\text{cryst}} + t_{\text{am}}$, where t_{am} is the thickness of the surface layers. When calculating t_{cryst} (the parameter required in calculations of the contrast), the intensity at zero crystal thickness (at the interface between the surface layer and the crystal) rather than that of vacuum was thus scaled to unity.²⁹

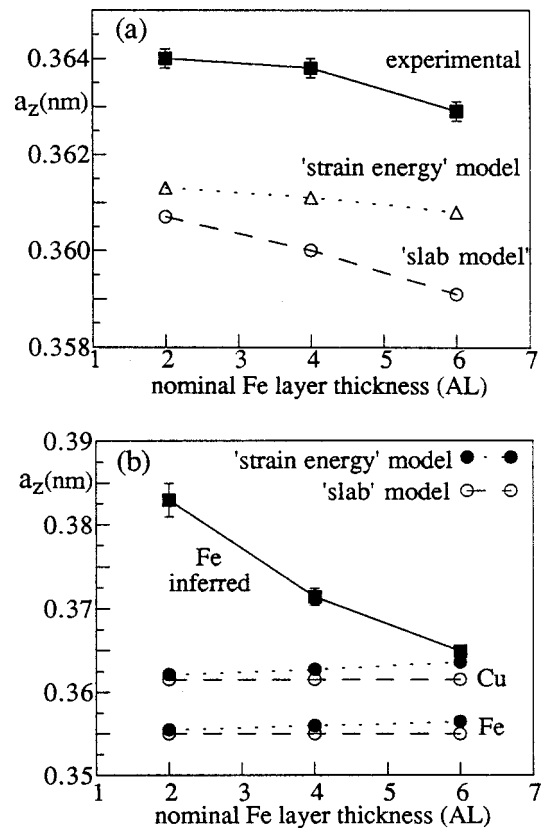


FIG. 5. (a) Average lattice parameter a_z along [001] for two models of multilayer structure and experimental (002) spacings. (b) a_z in Cu and Fe layers for two models of multilayer structure, and a_z in Fe inferred from experimental average a_z (assuming nominal thicknesses of Fe and Cu layers and a_z in Cu of 0.3615 nm).

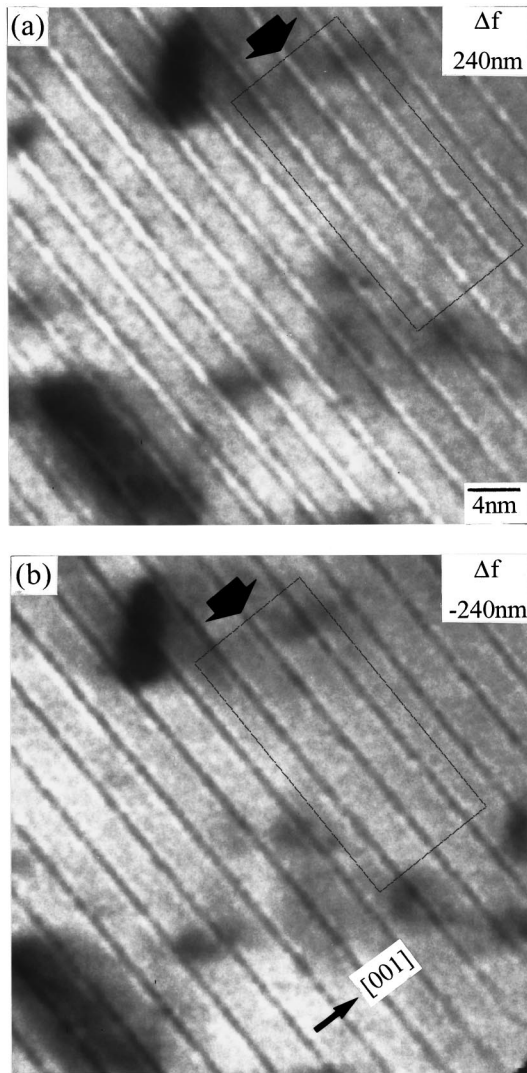


FIG. 6. Bright-field images of multilayer A at defocus values of 240 and -240 nm. The intensity in the boxed regions was projected in the arrowed direction to obtain line profiles.

Figure 6 shows two of the images obtained from multilayer A at measured defocus values of 240 and -240 nm. The sense of the reversal in contrast with defocus is consistent with the Fe layers having a higher scattering potential than Cu,²⁷ with the potential defined to be positive in the specimen relative to vacuum. Regions exhibiting uniform layer contrast were extracted from each such image, and the intensity was projected parallel to the layers over 300 pixels to form line profiles. These were divided by a smooth background, and the contrast from adjacent layers was averaged to increase the signal to noise ratio. The final one-dimensional line profiles are shown in Fig. 7 for one data set from each multilayer. The best-fitting simulated profiles, which were obtained using one-dimensional multislice calculations²⁷ for measured values of t_{cryst} (see Table IV below), are also shown. A Simplex algorithm³⁰ was used to vary the width, depth, and shape of the potential profile in the simulations iteratively, while also refining the experimental beam convergence and starting defocus value.³¹ Different starting parameters were used to verify that the solu-

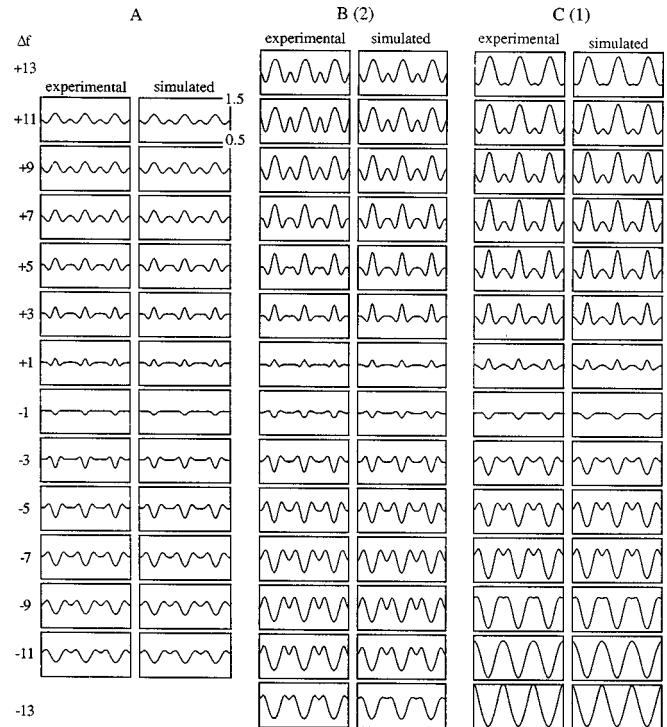


FIG. 7. Experimental and best-fitting simulated Fresnel contrast profiles for one data set from each multilayer. Defocus steps are 81 nm. The intensity scale is identical for all profiles.

tions correspond to global minima. The imaginary part of the scattering potential, which will be discussed below, was also fitted in the form of a constant fraction of the real part of the potential.

The match between the experimental and simulated profiles in Fig. 7 is excellent. The best-fitting potential profiles are shown in Fig. 8, averaged profiles from the data sets for each multilayer are shown in Fig. 9, and the best-fitting parameters are given in Table IV. The fitted potential profiles are all diffuse in shape, with a slight increase in width from A to B to C. The spread in the values of the potential difference ΔV between Fe and Cu for the same multilayer reflects both the accuracy to which the specimen thickness has been measured and the effect of varying degrees of compositional

TABLE IV. Best fits to Fresnel contrast data. Magnitudes of changes in potential at Fe layers and full widths at half maximum are labeled as ΔV and fwhm, respectively. α is the beam convergence semiangle.

Sample	Measured values			Best-fitting values			
	t (nm)	t_{cryst} (nm)	α (mrad)	α (mrad)	ΔV_{real} (V)	FWHM (nm)	ΔV_{imag} (V)
A	77	59	0.50	0.52	0.93	0.71	0.085
B(1)	70	43	0.49	0.39	1.72	0.92	0.011
B(2)	42	32	0.14	0.29	2.63	0.77	0.010
B(3)	31	22	0.17	0.23	1.98	0.71	0.031
B (mean)	-	-	-	-	2.11	0.80	0.017
C(1)	55	43	0.24	0.35	2.99	0.92	0.181
C(2)	71	55	0.19	0.27	3.29	0.98	0.014
C (mean)	-	-	-	-	3.14	0.95	0.098

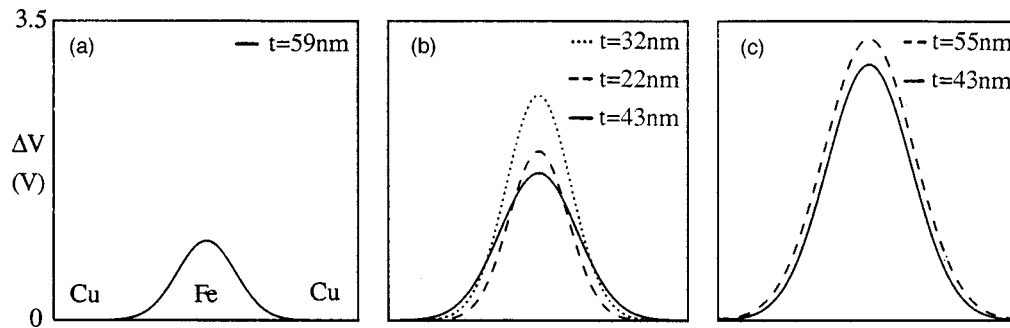


FIG. 8. Best-fitting potential profiles corresponding to one multilayer period, with value for Cu scaled to zero. (a) A, (b) B, (c) C.

averaging through the foil thickness. A further error in ΔV of around 10% may result from an incorrect choice of λ_{in} ; however this will not affect the trend in ΔV as a function of Fe-layer thickness. It should also be noted that the contribution to the contrast from magnetization of the Fe will be negligible as the objective lens will saturate the magnetization of the layers parallel to the electron beam.

V. INTERPRETATION

Electron-scattering factors $f_{el}(0)$ calculated by Doyle and Turner³² and more recently by Rez, Rez, and Grant in Ref. 33 are listed for Fe and Cu in Table V. The values for Fe from the two sources are similar; however, it is surprising that those for Cu are different. The true scattering factors may also differ from the calculated free atom values as a result of bonding and charge transfer. Given these uncertainties, the measured mean inner potential profiles will be interpreted using the scattering factors of both Doyle and Turner (DT) and Rez, Rez, and Grant (RRG).³⁴ Electron energy loss spectroscopy (EELS) will be used to provide an independent measure of the electron structures of the multilayers, and an estimate of layer ‘‘roughness’’ will be determined from the intensities of low-angle x-ray-diffraction superlattice lines.

A. Electron-energy-loss spectroscopy

Figure 10(a) shows electron-energy-loss spectra from the multilayers, in which systematic changes in the Fe white-line intensity and L_3/L_2 ratio are visible with layer thickness.³⁵ The L_3/L_2 ratios from the multilayers lie between those for

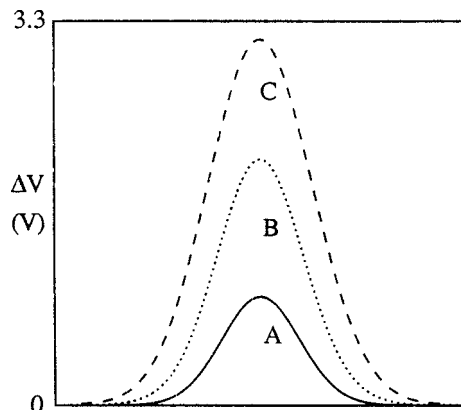


FIG. 9. Averaged potential profiles from data sets obtained from each multilayer.

bulk fcc and body-centered-cubic Fe.³⁶ The Cu spectra in Fig. 10(b) show no evidence of the formation of a white line, and are identical to pure bulk Cu, indicating that the Cu d band in the multilayers is full.³⁷ The decrease in Fe white-line intensity and L_3/L_2 ratio with increasing layer thickness cannot be associated with the formation of an ‘‘alloy’’ phase at the interfaces,³⁸ since this would require electron transfer from Fe to Cu. The Cu d band is full, and this charge could only be accommodated in the Cu $4s$ band, which is much broader than the $3d$ band and so could not accommodate the charge transfer suggested by the spectra without greatly increasing the energy of the transferred electrons. The changes in white line intensity (and thus electron structure) with Fe-layer thickness are better understood to be associated with lattice spacing changes in the Fe. If the (002) spacing in the Cu is assumed to correspond to the bulk cubic value, then the strain in the Fe (relative to its cubic lattice parameter) is inferred to be 6.8%, 3.6%, and 1.8% for A, B, and C, respectively [see Fig. 5(b)]. This correlates closely with the changes in white line intensity in Fig. 10(a).

B. Roughness

Both the EELS data and the mutual insolubility of Fe and Cu suggest that the Fe/Cu interface structure is better described as roughness than as interdiffusion. On a larger scale, fluctuations in layer width will broaden a measured potential profile if their characteristic length scale is smaller than the foil thickness. The potential profiles from multilayer B do indeed show an increase in full width at half maximum (fwhm) with increasing foil thickness. The fwhm of the profile from C is similar to its nominal width of six AL’s, suggesting that the middle layers are pure Fe in projection and that the amplitude of any roughness is less than about two AL’s.

An independent estimate of layer roughness may be inferred from the low-angle x-ray superlattice lines shown in Fig. 11, by analogy with the decrease in x-ray intensity with

TABLE V. Electron scattering factors at zero scattering angle $f_{el}(0)$ in nm from calculations of Doyle and Turner (Ref. 32) (DT) and Rez, Rez, and Grant (Ref. 33) (RRG).

	DT	RRG
Fe	0.7165	0.71403
Cu	0.5600	0.62851

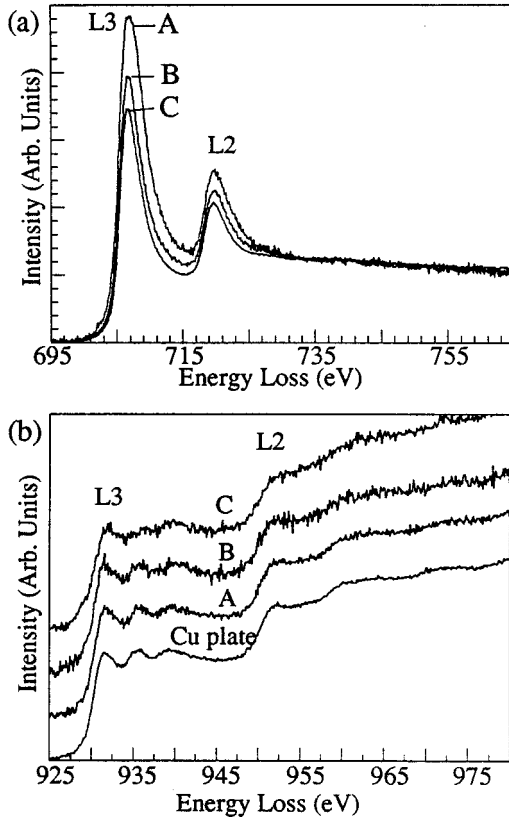


FIG. 10. Background-subtracted (a) Fe and (b) Cu L edges from electron-energy-loss spectra, with Fe edges normalized to the continuum after the edge. The spectrum obtained from the Cu plate is also shown in (b). Specimen foils were sufficiently thin for multiple scattering to be negligible, so spectra were not deconvoluted.

increasing angle due to thermal vibrations.³⁹ This may be modelled using a Debye-Waller factor⁴⁰

$$DW = \exp\left(\frac{-16\pi^2\sigma^2\sin^2\theta}{\lambda^2}\right), \quad (4)$$

where σ is the root-mean-square “roughness” at the interfaces, and λ is the x-ray wavelength. Taking account of the decay in reflectivity with angle θ , the satellite intensities obey the equation

$$\frac{I}{I_0} = \frac{C}{\sin^3\theta} \exp\left(\frac{-16\pi^2\sigma^2\sin^2\theta}{\lambda^2}\right), \quad (5)$$

where C is a constant. The values of σ determined using this approach are 0.12, 0.21, and 0.24 nm (0.7, 1.2, and 1.3 AL's) for multilayers, A, B, and C, respectively, suggesting that the roughness of multilayer A would be overestimated on the assumption that it is similar to that of C.

Roughnesses much greater than two AL's are required to fit the measured potential profiles if changes in lattice spacing are not included in the model. Conversely, strains much greater than can be reconciled with the x-ray measurements are required to fit the data. Hence both compositional and spacing changes must be included in the model. Figure 12 shows the results of such a model for values of ε_{Fe} inferred from the experimental x-ray data and roughness amplitudes

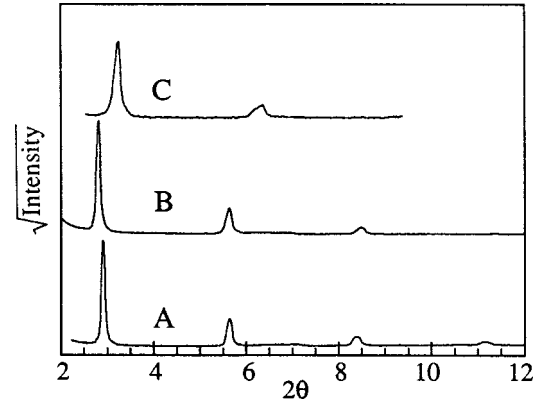


FIG. 11. Low-angle x-ray superlattice lines for multilayers A, B, and C, offset for clarity.

of between one and two AL's. To within experimental error, the measured and calculated values of ΔV agree if RRG scattering factors are used.

C. Areas under the potential profiles

The area beneath the potential barrier associated with an Fe layer is given by the equation

$$S = \Delta V n \frac{a_z^{\text{Fe}}}{2} \equiv \frac{2kn}{a_x^2} \left(f_{\text{el}}^{\text{Fe}}(0) - \frac{f_{\text{el}}^{\text{Cu}}(0)a_z^{\text{Fe}}}{a_z^{\text{Cu}}} \right), \quad (6)$$

where n is the number of planes of Fe. Values of S for each sample are listed in Table VI. The spread in S for the different data sets from multilayer B is less than that in ΔV , suggesting that some of the variation in ΔV is due to different amounts of through-thickness compositional averaging. Figure 13 shows that the strain in the Fe inferred from the values of S is also consistent with calculations that include RRG scattering factors.

An independent estimate of the ratio of Fe to Cu was obtained using energy-dispersive x-ray analysis (EDX), as the nominal layer thicknesses were determined from the deposition conditions and may be in error by up to ~5% and ~15% because of variations in sputtering power and erosion

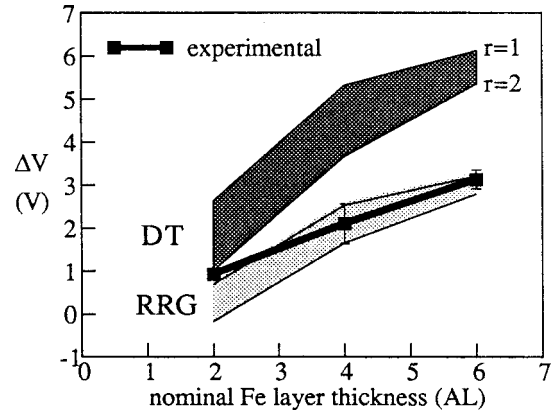


FIG. 12. Comparison of experimental ΔV with a model that includes Fe strains inferred from x-ray-diffraction data, for composition profiles smoothed using Gaussians with root-mean-square radii (r) of between one and two AL's. The calculation was for a common in-plane lattice parameter a_x of 0.36 nm and a lattice parameter parallel to $[001]$ a_z^{Cu} of 0.3615 nm.

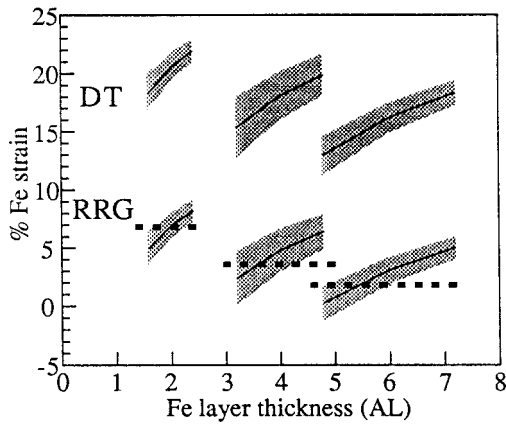


FIG. 13. (002) strain in Fe layers calculated from areas under potential, assuming that Cu retains its cubic lattice parameter, compared to strain inferred from x-ray-diffraction data (dashed line). Shaded regions correspond to the uncertainty in the layer width and S .

of the target, respectively. Table VII shows the Fe layer thicknesses calculated both on the basis of the raw EDX data and after correction by subtracting a hole count.⁴¹ The value for multilayer C (from which the data should be more reliable given the higher proportion of Fe) is close to the nominal layer thickness of six AL's. However, the ratio of S for the different multilayers does not fit the ratio determined by EDX, providing further evidence that the data cannot be explained on a purely compositional basis.

D. Scattering factors and charge transfer

A good fit to the measured potential profiles has been obtained using RRG scattering factors. However, the scattering factor for Cu was calculated for a $3d^94s^2$ free-atom configuration by RRG,⁴² and a $3d^{10}4s^1$ configuration by DT. EELS spectra show that the d band in the Cu is full, and hence the DT value should be the more realistic of the two. A scattering factor for Fe lower than that predicted by both RRG and DT is thus required to fit the experimental values of ΔV and S . This would be the case if the scattering factor for Fe were similar to that of a free atom with a $3d^74s^1$ electron configuration rather than $3d^64s^2$. The scattering factor for a $3d^74s^1$ configuration is 0.633 nm,⁴³ corresponding to a difference in scattering factors between Fe and Cu of 0.07 nm, which is very close to the value of 0.09 nm used in the analysis above.

TABLE VI. Areas (S) under potential profiles.

Sample	S (nm V)	S ratio
A	0.70	1.0
B(1)	1.71	2.4
B(2)	2.18	3.1
B(3)	1.50	2.1
B (mean)	1.80	2.6
C(1)	2.92	4.2
C(2)	3.40	4.8
C (mean)	3.16	4.5

Further evidence that the Fe-scattering factors are different from free-atom values is provided by the imaginary part of the scattering potential (see Table IV), which is positive for all three multilayers and indicates that the Fe scatters more to high angles than the Cu. Electron-scattering factors for Fe and Cu are shown as a function of scattering angle in Fig. 14. In contrast to the experimental data, integrating over angles greater than the objective aperture radius used for the Fresnel contrast measurements suggests that the absorptive potential should be negative. Calculations⁴⁴ using the routines of Weickenmeier and Kohl⁴⁵ also indicate that there should be more thermal diffuse scattering to the relevant angles from Cu. However, it would only require a small change in the Debye-Waller factors (which are structure sensitive) or the scattering factors (which are sensitive to the distribution of outer electrons) for the calculation to agree with the data.

The change in the scattering factor of Fe may be associated partly with the redistribution of d band electrons. EELS showed effects related to changes in d -band occupancy and the distribution of $d_{5/2}$ and $d_{3/2}$ states. Such changes would be related to the magnetic moments of the layers and would have analogies with the Weiss two-states model of fcc Fe, in which two structures (high spin, high volume, ferromagnetic and low spin, low volume, antiferromagnetic) are related by the spin flip of one electron.⁴⁶

Huberman and Grimsditch⁴⁷ suggested that the Fermi energies of thin metal films would equalize through changes in lattice spacing. A revision of the model⁴⁸ predicted that the lattice spacings would change to move the Fermi levels in the two metals further apart. For $E_f(\text{Fe}) > E_f(\text{Cu})$ the Fe would contract, the Cu expand, and charge would be transferred from Fe to Cu, while for $E_f(\text{Cu}) > E_f(\text{Fe})$ the Fe would expand, the Cu contract, and charge would be transferred from Cu to Fe. Although the latter configuration of Fermi energies would agree with the observed expansion in the Fe, it is not consistent with the direction of charge transfer indicated by EELS.

The observed electron structure modifications may be associated with the presence of quantum-well states in the layers. Calculations using a free-electron model predict large changes in the Fermi energies and densities of states of thin layers relative to bulk values,⁴⁹ and there is experimental evidence for quantum size effects in metallic thin films.⁵⁰ The effect of quantum-well states on interlayer coupling in metallic multilayers has been considered,⁵¹ and a similar modeling is required to determine their effect on *structure*. In the past, the interaction between the Fermi surface and the additional Brillouin zones arising from the multilayer periodicity have been used to explain the supermodulus effect² and structural anomalies.⁵² These additional Brillouin zones must be present in the multilayers examined here; however, they cannot be the primary cause of the trend in Fe(002) spacing with layer thickness since Λ is similar for each multilayer. In future studies, it will also be important to determine the relationship between potentials measured by high-energy electrons⁵³ and conduction electrons. This may allow electron microscopy to provide insight into giant magnetoresistance⁵⁴ and other multilayer properties.

TABLE VII. Compositional characterization of multilayers from EDX data, assuming a nominal Fe (002) spacing of 0.181 nm and Λ determined using x-ray diffraction. (Calculated K factors were used; it was not possible to determine experimental K factors because Fe and Cu do not alloy).

Sample	Nominal w_{Fe} (nm)	Original EDX w_{Fe} (nm)	Corrected EDX w_{Fe} (nm)	Original EDX ratio	Corrected EDX ratio
A	0.36 ± 0.07	0.23	0.29	1.0	1.0
B	0.72 ± 0.14	0.46	0.51	2.0	1.8
C	1.09 ± 0.22	0.87	1.03	3.7	3.6

E. A tetragonal Fe phase

Our results show that the Fe is ferromagnetic with $c/a > 1$, whereas calculations of the stability of *bulk-tetragonal* Fe phases⁵⁵ suggest that the lowest-energy fct structure is antiferromagnetic with $c/a < 1$. The structure cannot be understood in terms of coherency strains,⁵⁶ since these would result in a contraction of the (002) spacings rather than the observed expansion. We suggest that the “stress-free” structure from which the Fe is distorted on forming a coherent multilayer is tetragonal with $c > a$, as illustrated schematically in Fig. 15. Calculations of elastic strain energy and magnetoelastic energy will thus be in error if cubic lattice parameters are assumed. Furthermore, the magnetic anisotropy that results in the magnetic easy axis

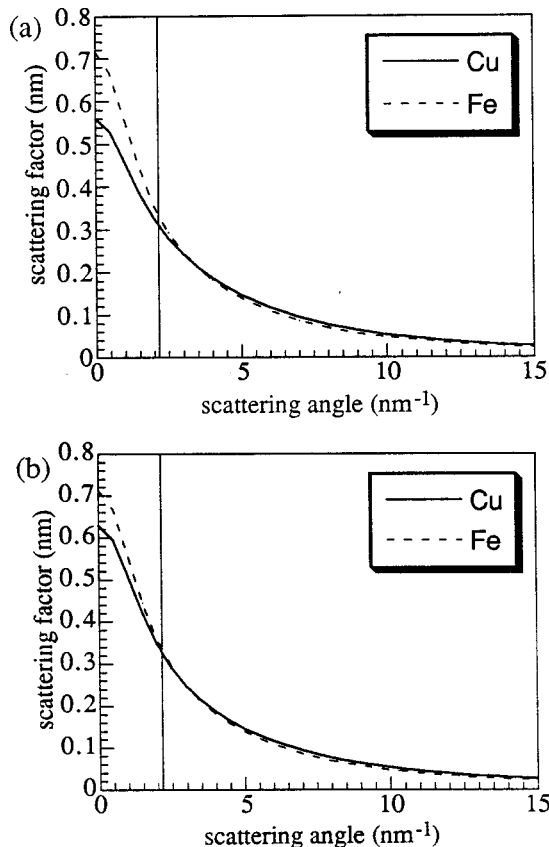


FIG. 14. (a) DT and (b) RRG scattering factors plotted as function of scattering angle, with the vertical line marking the objective aperture radius used for obtaining Fresnel contrast data.

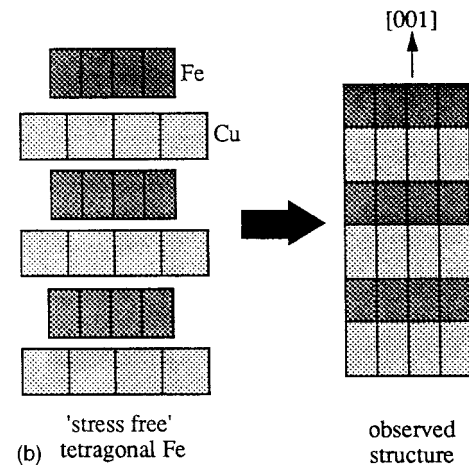
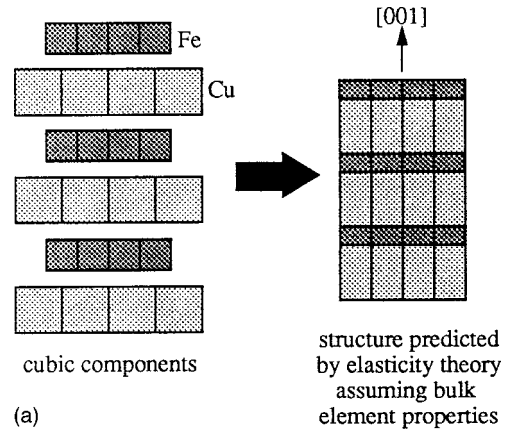


FIG. 15. Schematic diagram illustrating the multilayer structure formed from (a) cubic Fe and Cu, and (b) tetragonal Fe ($c > a$) and cubic Cu.

lying parallel to the layer normal may not simply be an interface effect, but may be explained by a thickness-dependent “bulk” anisotropy.⁵⁷

The identification of tetragonal phases with elastic anomalies in metals contrasts with the behavior of semiconductor multilayers, whose structures are consistent with conventional elasticity theory⁵⁸ and display no elastic anomalies.⁵⁹ This difference may result from the fact that bonding bands in semiconductors are full and there is no energy gain in reducing the symmetry of the structure, in contrast to Jahn-Teller-type distortions in *atomic* complexes with unfilled electron shells.⁶⁰ In this context, it is interesting to note that α -Sn (which has a band gap between bonding and antibonding states) is cubic, whereas β -Sn is metallic and tetragonal. Tetragonal metallic Si and Ge structures can also be stabilized at high pressures.⁶¹ Furthermore Cu/Au superlattices, in which both components have full d bands, do not show anomalous properties,⁶² and in the multilayers examined here the Cu layers behave identically to the bulk material.

A stable stress-free tetragonal phase may explain certain observations in other metal multilayers. For example, in the Fe/Ir system the Fe is body-centered-tetragonal (bct),⁶³ and decreases in tetragonality with increasing layer thickness, suggesting that the bct phase is not a “precursor” to the higher volume bcc structure. Tetragonal phases may also ac-

count for anomalous lattice spacings observed in Cu/NiPd multilayers,⁵² changes in strain with layer thickness and Λ in Cu/Pd multilayers⁶⁴ and other observations that it is difficult to rationalize using models that associate the anomalous behavior with the interfaces.⁶²

VI. CONCLUSIONS

(1) The (002) spacings in three crystalline Fe/Cu multilayers are not consistent with the predictions of conventional elasticity theory if bulk elastic constants and lattice parameters are used. The Fe(002) spacings are expanded relative to their cubic value by 6.8%, 3.6%, and 1.8% for Fe-layer thicknesses of two, four, and six AL's, respectively. We suggest that the unstrained lattice parameter of Fe is thickness dependent and tetragonal with $c > a$.

(2) The electron structure of the Fe is layer thickness dependent, and is similar to that of a free atom with a $3d^74s^1$ rather than a $3d^64s^2$ electron configuration. In contrast, the Cu layers behave like the bulk material.

(3) The model of Huberman and Grimsditch⁴⁸ is not consistent with our results.

(4) A characterization of the type described here, combined with *ab initio* modeling to determine the effects of electron structure distortions on atomic structure, is essential for understanding and tailoring the properties of such synthetic nanostructures.

ACKNOWLEDGMENTS

Dr. R. E. Somekh is thanked for his assistance with the deposition of the multilayers, Dr. P. Rez for calculating electron scattering factors for Fe and Cu for several electron configurations, and Dr. C. B. Boothroyd and Dr. A. R. Preston for discussions. The financial support of the EPSRC (S.J.L. and R.D.B.) and Trinity Hall, Cambridge (S.J.L.) is gratefully acknowledged. Finally, the authors acknowledge the inspiration and guidance of the late Dr. W. M. Stobbs.

APPENDIX A

In the slab model, the strain in the iron parallel to [001] is given by

$$\varepsilon_3 = 2\varepsilon_1 \left(\frac{S_{12}}{S_{11} + S_{12}} \right), \quad (\text{A1})$$

where

$$\varepsilon_1 = \left(\frac{a_{\text{Fe}} - a_{\text{Cu}}}{a_{\text{Cu}}} \right), \quad (\text{A2})$$

S_{11} and S_{12} are elastic compliances in standard matrix notation, and a_{Fe} and a_{Cu} are bulk lattice parameters.

In the strain energy model, the elastic strain energy per unit volume, W , is minimized. W is given by the tensor equation

$$W = C_{ij} \varepsilon_i \varepsilon_j, \quad (\text{A3})$$

where C_{ij} is the stiffness tensor, and ε_i and ε_j are strain matrices. For biaxial strain in multilayers whose normal is [001], this equation simplifies to

$$W = (C_{11} + C_{12}) \varepsilon_1^2, \quad (\text{A4})$$

where, for the Fe (and similarly for the Cu) layers,

$$\varepsilon_1^{\text{Fe}} = \left(\frac{a_{\text{Fe}} - a_x}{a_x} \right). \quad (\text{A5})$$

The common in-plane lattice parameter

$$a_x = \left(\frac{a_{\text{Cu}}^2 w_{\text{Cu}} (C_{11}^{\text{Cu}} + C_{12}^{\text{Cu}}) + a_{\text{Fe}}^2 w_{\text{Fe}} (C_{11}^{\text{Fe}} + C_{12}^{\text{Fe}})}{a_{\text{Cu}} w_{\text{Cu}} (C_{11}^{\text{Cu}} + C_{12}^{\text{Cu}}) + a_{\text{Fe}} w_{\text{Fe}} (C_{11}^{\text{Fe}} + C_{12}^{\text{Fe}})} \right), \quad (\text{A6})$$

where w is the thickness of each layer. The strain ε_3 may then be calculated using Eq. (A1).

APPENDIX B

λ can be calculated using the relation

$$\lambda_{\text{in}} \approx \frac{106F(E_0/E_m)}{\ln(2\beta E_0/E_m)}, \quad (\text{B1})$$

where $F = 0.4397$ at 397 kV. E_0 is the accelerating voltage in kV, β is the objective aperture semiangle in mrad and the mean energy loss in V, and

$$E_m \approx 7.6Z^{0.36}, \quad (\text{B2})$$

where Z is the atomic number.²⁸ E_m and λ_{in} for Cu are calculated to be 25.5 eV and 155 nm, respectively. However, measurements suggest that $E_m = 30.8$ eV, corresponding to a value for λ_{in} of 134 nm. For Fe, E_m calculated using Eq. (B2) is 24.6 eV, which is close to the experimental value and corresponds to a λ_{in} of 160 nm. It is reasonable to assume that increasing the Fe content of the multilayer will increase λ_{in} . However, Eq. (B1) is only valid for $\beta \ll (E/E_0)^{1/2}$. For large collection angles, λ_{in} saturates at a value independent of β , suggesting that for the present experimental conditions λ_{in} is overestimated using Eq. (B1). Taking all of these considerations into account, a value for λ_{in} of 130 nm will be used for the multilayers.

*Present address: Center for Solid State Science, Arizona State University, Tempe, AZ 85287-1704.

¹F. Capasso, *Science* **235**, 172 (1987).

²R. W. Cahn, *Nature (London)* **324**, 108 (1986).

³*Ultrathin Magnetic Structures*, edited by J. A. C. Bland and B. Heinrich (Springer-Verlag, Berlin, 1994), Vols. I and II.

⁴E. E. Fullerton, I. K. Schuller, F. T. Parker, K. A. Svinarich, G. L.

Eesley, R. Bhadra, and M. Grimsditch, *J. Appl. Phys.* **73**, 7370 (1993).

⁵G. A. Prinz, *J. Magn. Magn. Mater.* **100**, 469 (1991).

⁶B. M. Clemens and G. L. Eesley, *Phys. Rev. Lett.* **61**, 2356 (1988).

⁷W. F. Egelhoff, in *Ultrathin Magnetic Structures* (Ref. 3).

⁸On the formation of a coherent multilayer from what are *conven-*

- tionally understood as cubic components, the symmetry of the structure within the individual layers is reduced to tetragonal as a result of atomic spacing changes associated with the constraint of coherent growth. While the conventional Bravais lattice of the material within each layer is body-centered-tetragonal, in order to preserve the simple relationship with the original cubic lattice a face-centered-tetragonal cell with c defined along the layer normal is referred to here.
- ⁹F. Yoshizaki, N. Tanaka, and K. Mihama, *J. Electron Microsc.* **39**, 459 (1990).
 - ¹⁰V. L. Moruzzi, P. M. Marcus, and J. Kubler, *Phys. Rev. B* **39**, 6957 (1989).
 - ¹¹G. J. Johanson, M. B. McGirr, and D. A. Wheeler, *Phys. Rev. B* **1**, 3208 (1970).
 - ¹²U. Gonser, K. Krischel, and S. Nasu, *J. Magn. Magn. Mater.* **15–18**, 1145 (1980).
 - ¹³D. Li, M. Freitag, J. Pearson, Z. Q. Qiu, and S. D. Bader, *J. Appl. Phys.* **76**, 6425 (1994).
 - ¹⁴B. Heinrich and J. F. Cochran, *Adv. Phys.* **42**, 523 (1993).
 - ¹⁵The sputtering conditions were to initially chosen favor nucleation processes to form a continuous Cu buffer (a low sputtering pressure of ~ 1 Pa and a low deposition rate of ~ 0.01 nm s⁻¹ were used). The multilayers were then grown at a higher sputtering pressure (~ 4.5 Pa) and a higher deposition rate (~ 0.1 nm s⁻¹), with the temperature reduced during deposition from ~ 470 to ~ 400 K. See R. E. Somekh and C. S. Baxter, *J. Cryst. Growth* **76**, 119 (1986).
 - ¹⁶S. J. Lloyd, R. E. Somekh and W. M. Stobbs, in *Metastable Phases and Microstructures*, edited by R. Bormann, G. Mazzone, R. S. Averback, R. D. Shull, and R. F. Ziolo, MRS Symposia Proceedings No. 400 (Materials Research Society, Pittsburgh, 1996), p. 317.
 - ¹⁷E. E. Fullerton, I. K. Schuller, H. Vanderstraeten, and Y. Bruynseraede, *Phys. Rev. B* **45**, 9292 (1992).
 - ¹⁸*Elastic, Piezoelectric, Piezooptic, Electrooptic, Constants, and Nonlinear Dielectric Susceptibilities of Crystals*, edited by K. H. Hellwege and O. Madelung, Landolt-Börnstein, New Series, Group III, Vol. 2 (Springer-Verlag, Berlin, 1969).
 - ¹⁹R. A. Johnson, *Phys. Rev.* **145**, 423 (1966).
 - ²⁰S. H. Lu, J. Quinn, D. Tian, and F. Jona, *Surf. Sci.* **209**, 364 (1989).
 - ²¹S. J. Lloyd, R. E. Somekh, and W. M. Stobbs in *Structure and Properties of Multilayered Thin Films*, edited by T. D. Nguyen, B. M. Lairson, B. M. Clemens, K. Sato, and S-C. Shin, MRS Symposia Proceedings No. 382 (Materials Research Society, Pittsburgh, 1995), p. 155
 - ²²C. S. Baxter and W. M. Stobbs, *Ultramicroscopy* **16**, 213 (1985).
 - ²³In high-energy electron diffraction, only the Coulomb potential needs to be considered since exchange and correlation effects are negligible (Refs. 24 and 25).
 - ²⁴D. K. Saldin and J. C. H. Spence, *Ultramicroscopy* **55**, 397 (1994).
 - ²⁵P. Rez, *Acta Crystallogr., Sect. A: Cryst. Phys., Diff., Theor. Gen. Crystallogr.* **34**, 48 (1978).
 - ²⁶See, e.g., P. B. Hirsch, A. Howie, R. Nicholson, D. W. Pashley, and M. J. Whelan, *Electron Microscopy of Thin Crystals*, 2nd ed. (Krieger, Florida, 1977).
 - ²⁷F. M. Ross and W. M. Stobbs, *Philos. Mag. A* **63**, 1 (1991); **63**, 37 (1991).
 - ²⁸R. F. Egerton, *Electron Energy-Loss Spectroscopy in the Electron Microscope*, 2nd ed. (Plenum, New York, 1996).
 - ²⁹R. E. Dunin-Borkowski, C. B. Boothroyd, S. J. Lloyd, and W. M. Stobbs, *J. Microsc.* **180**, 263 (1995).
 - ³⁰W. H. Press, B. P. Flannery, S. A. Teukolsky, and W. T. Vetterling, *Numerical Recipes* (Cambridge University Press, Cambridge, 1989).
 - ³¹R. E. Dunin-Borkowski (unpublished).
 - ³²P. A. Doyle and P. S. Turner, *Acta Crystallogr., Sect. A: Cryst. Phys., Diff., Theor. Gen. Crystallogr.* **24**, 390 (1968).
 - ³³D. Rez, P. Rez, and I. Grant, *Acta Crystallogr., Sect. A: Found. Crystallogr.* **50**, 481 (1994).
 - ³⁴Only after considering the possible contributions to the observed values of ΔV is it possible to assess which, if either, of the two sets of scattering factors are the more appropriate. If the other parameters affecting the value of ΔV can be determined independently, then an analysis of the Fresnel contrast may in principle be used to determine the true scattering factors, and hence to infer the electron distribution within the multilayer.
 - ³⁵The white lines result from the excitation of p electrons into d -band empty states, and are sensitive to crystal structure, lattice spacing, local charge transfer, and magnetic moment. See S. J. Lloyd, G. A. Botton, and W. M. Stobbs, *J. Microsc.* **180**, 288 (1995).
 - ³⁶S. J. Lloyd, G. A. Botton, and W. M. Stobbs, *Inst. Phys. Conf. Ser.* **147**, 31 (1995).
 - ³⁷D. H. Pearson, C. C. Ahn, and B. Fultz, *Phys. Rev. B* **50**, 12969 (1994).
 - ³⁸The concept of “charge transfer” associated with alloying is controversial. See for example, *Theory of Alloy phase formation*, edited by L. H. Bennett (AIME, Warrendale, PA, 1980). Here only the possibility that the changes in the white lines could be explained by some form of charge redistribution between the alloy components is considered.
 - ³⁹B. D. Cullity, *Elements of X-ray Diffraction*, 2nd ed. (Addison-Wesley, Reading MA, 1978).
 - ⁴⁰E. Spiller and A. E. Rosenbluth, *Proc. SPIE* **563**, 221 (1985).
 - ⁴¹The hole count was given by positioning the probe away from the foil edge and measuring the Cu signal. It is generated by stray scattering from the column generating x rays from the Cu surrounding the multilayer, and a further underestimate of the Fe content may result from the surface layer of sputter on the sample. See M. H. Loretto, *Electron Beam Analysis of Materials*, 2nd ed. (Chapman & Hall, London, 1994).
 - ⁴²P. Rez has since calculated a scattering factor for Cu with a $3d^{10}4s^1$ configuration, which is very similar to the DT value.
 - ⁴³P. Rez (private communication).
 - ⁴⁴A. R. Preston (private communication).
 - ⁴⁵A. Weickenmeier and H. Kohl, *Acta Crystallogr. Sect. A: Found. Crystallogr.* **47**, 590 (1991).
 - ⁴⁶R. J. Weiss, *Proc. Phys. Soc. London* **82**, 281 (1963).
 - ⁴⁷M. L. Huberman and M. Grimsditch, *Phys. Rev. Lett.* **62**, 1403 (1989).
 - ⁴⁸M. L. Huberman and M. Grimsditch, *Phys. Rev. B* **46**, 7949 (1992).
 - ⁴⁹J. P. Rogers III, P. H. Cutler, T. E. Feuchtwang, and A. A. Lucas, *Surf. Sci.* **181**, 436 (1987).
 - ⁵⁰M. Jalochofski, *Prog. Surf. Sci.* **48**, 287 (1995).
 - ⁵¹C. Sommers and P. M. Levy, *J. Phys. (France)* **6**, 1461 (1996).
 - ⁵²C. S. Baxter and W. M. Stobbs, *Nature (London)* **322**, 814 (1986).
 - ⁵³M. O’Keefe and J. C. H. Spence, *Acta Crystallogr., Sect. A: Found. Crystallogr.* **50**, 33 (1994).

- ⁵⁴M. D. Stiles, Phys. Rev. B **48**, 7238 (1993).
- ⁵⁵S. S. Peng and H. J. F. Jansen, Ultramicroscopy **47**, 361 (1992).
- ⁵⁶D. Li, M. Freitag, J. Pearson, Z. Q. Qiu, and S. D. Bader, Phys. Rev. Lett. **72**, 3112 (1994).
- ⁵⁷W. J. M. de Jonge, P. J. H. Bloemen, and F. J. A. den Broeder, in *Ultrathin Magnetic Structures* (Ref. 3).
- ⁵⁸J. E. Bernard and A. Zunger, Appl. Phys. Lett. **65**, 165 (1994).
- ⁵⁹M. Grimsditch, R. Bhadra, I. K. Schuller, F. Chambers, and G. Devane, Phys. Rev. B **42**, 2923 (1990).
- ⁶⁰A. Cottrell, *Introduction to the Modern Theory of Metals* (Institute of Metals, London, 1988).
- ⁶¹J. C. Jamieson, Science **139**, 762 (1963).
- ⁶²M. Grimsditch, Superlattices Microstruct. **4**, 677 (1988).
- ⁶³S. Andrieu, J. Hubsch, M. Piecuch, L. Hennet, and H. Fischer, in *Magnetic Ultrathin Films, Multilayers and Surfaces Interfaces and Characterization*, edited by B. T. Jonker, S. A. Chambers, R. F. C. Farrow, C. Chappert, R. Clarke, W. J. M. de Jonge, T. Egami, P. Grünberg, K. M. Krishnan, E. E. Marinero, C. Rau, and S. Tsunashima, MRS Synposia Proceedings No. 313 (Materials Research Society, Pittsburgh, 1993), p. 473.
- ⁶⁴T. Ueda, G. F. Simenson, W. D. Nix, and B. M. Clemens, in *Structure and Properties of Multilayered Thin Films* (Ref. 21), p. 279.